Project 1 Solution: Flow in a Diffuser

AERO 523 Fall 2021
Author: Erik Rutyna

October 1, 2021

Introduction

The goal of this project was to solve for the flow field over half a diffuser for an incompresible and irrotational flow using the Finite Difference Method (FDM). Since this problem existed in 2-D, the flow can be modelled using a 2-D stream function, $\psi(x, y)$, over the domain shown in Figure 1 [2]. Only half of the diffuser is used as the diffuser is mirror over the x-axis. Figure 1 shows this diffuser along with how to calculate its geometry and boundary conditions.

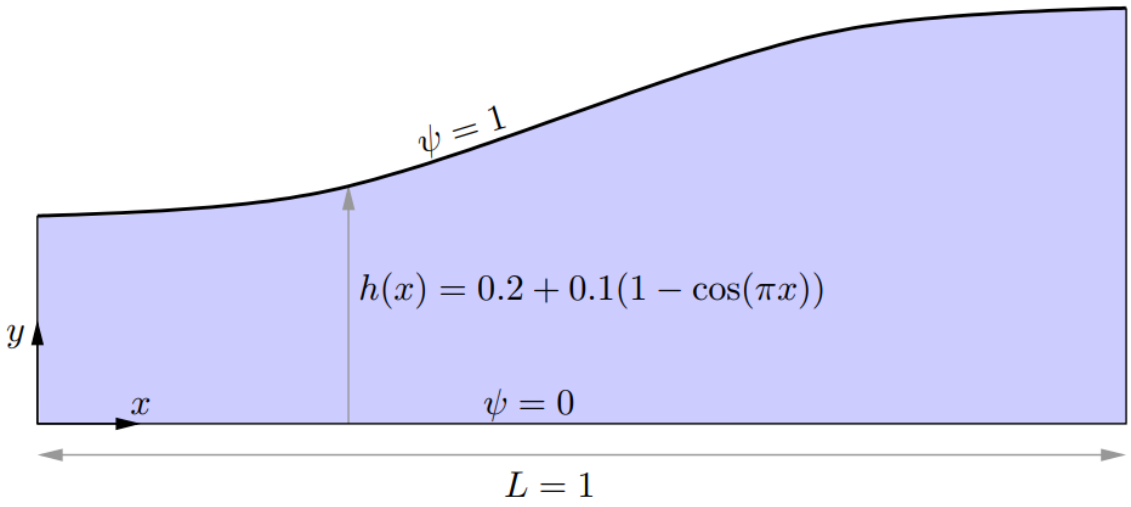

Figure 1: A visualization of half of the diffuser that is used as our domain.

This stream function, $\psi(x, y)$, has velocity components that can be found by taking the following partial derivatives

$$u = \frac{\partial \psi}{\partial y}, \quad v = -\frac{\partial \psi}{\partial x}, \tag{1}$$

and this definition coupled with our other assumptions leads to Laplace's equation for $\psi(x, y)$,

$$\nabla^2 \psi = 0, \tag{2}$$

which can then be discretized across the domain such that ψ can be solved for.

Setup (Task 1 - Mapping)

The governing equation of the flow in our domain is shown in Eqn. 2, and it can be expanded to become

$$\frac{\partial^2 \psi}{\partial x^2} + \frac{\partial^2 \psi}{\partial y^2} = 0. \tag{3}$$

The form in Eqn. 3 is easier to discretize than that of Eqn. 2 as it is now known which derivatives need to taken. However, due to the non-uniform nature of the domain in the global space, it is easier to normalize the domain into a unit reference square domain shown in Figure 2. Here the FDM can be applied with ease due to the constant spacing in both ξ and η directions.

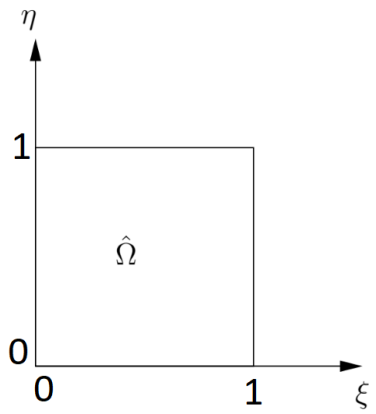

Figure 2: The unit square reference domain

Domain Normalization

The simplest way to normalize the domain into a uniform square with unit length on each side is to normalize the coordinates in the global domain by themselves. Figure 1 shows the relationships for the x-axis and y-axis. In this case the geometry is a function of x, so x gets to be an independent variable and can be transformed into reference space directly via

$$\xi = x. \tag{4}$$

The y-coordinate requires an additional step since the height is a function of the x coordinate. The y-coordinate can be normalized by the height function to get

$$\eta = \frac{y}{h(x)}. \tag{5}$$

Domain Discretization & Refinement

The reference domain is broken into a uniform grid of points that vary in quantity depending on if one is looking along the ξ-axis or the η-axis. In the ξ-direction there are $N_\xi = (4N + 1)$ points, and in the η-direction there are $N_\eta = (N + 1)$ points, where $N = 2^{2+r}$, and where $r \equiv$ the refinement index. The total number of grid points is then $N_{tot} = N_\xi \cdot N_\eta$. The global and reference domains have been plotted for $r = 0$ and can be seen in Figures 3a and 3b, respectively.

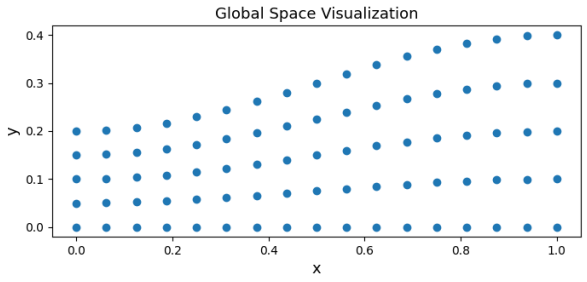

(a) Visualization of the global domain where contours are plotted.

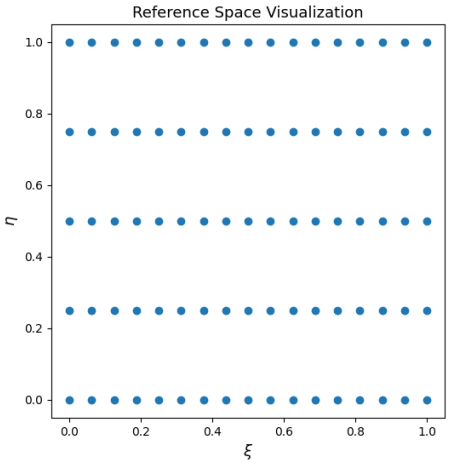

(b) Visualization of the reference domain where computations are done.

In order to plot contour mappings of various properties in the global domain, the location of points in the reference domain is mapped back to the global domain by the inverse of the previously established mapping. In the case of x, the inverse is the same function as the mapping, but for y, it needs to be multiplied by $h(x)$ to get

$$y = \eta \cdot h(x). \tag{6}$$

Task 1 - Reference Derivatives & Discretization

The formulas to discretize Eqn. 3 in the reference domain are [1]

$$\psi_{xx} = \psi_{\xi\xi}\xi_x^2 + 2\psi_{\xi\eta}\xi_x\eta_x + \psi_{\eta\eta}\eta_x^2 + \psi_\xi\xi_{xx} + \psi_\eta\eta_{xx} \tag{7}$$

and

$$\psi_{yy} = \psi_{\xi\xi}\xi_y^2 + 2\psi_{\xi\eta}\xi_y\eta_y + \psi_{\eta\eta}\eta_y^2 + \psi_\xi\xi_{yy} + \psi_\eta\eta_{yy}. \tag{8}$$

Now the PDE can be discretized with respect to reference space coordinates. Applying a second order accurate formula for both the first and second derivatives one receives

$$\begin{aligned}\psi_{xx} =& \frac{\psi_{i-1,j} - 2\psi_{i,j} + \psi_{i+1,j}}{\Delta\xi^2}\xi_x^2 + \\ & 2\frac{\psi_{i-1,j-1} + \psi_{i+1,j+1} - \psi_{i-1,j+1} - \psi_{i+1,j-1}}{4\Delta\xi\Delta\eta}\xi_x\eta_x + \\ & \frac{\psi_{i,j-1} - 2\psi_{i,j} + \psi_{i,j+1}}{\Delta\eta^2}\eta_x^2 + \\ & \frac{\psi_{i+1,j} - \psi_{i-1,j}}{\Delta\xi}\xi_{xx} + \frac{\psi_{i,j+1} - \psi_{i,j-1}}{\Delta\eta}\eta_{xx},\end{aligned} \tag{9}$$

and

$$\begin{aligned}\psi_{yy} =& \frac{\psi_{i-1,j} - 2\psi_{i,j} + \psi_{i+1,j}}{\Delta\xi^2}\xi_y^2 + \\ & 2\frac{\psi_{i-1,j-1} + \psi_{i+1,j+1} - \psi_{i-1,j+1} - \psi_{i+1,j-1}}{4\Delta\xi\Delta\eta}\xi_y\eta_y + \\ & \frac{\psi_{i,j-1} - 2\psi_{i,j} + \psi_{i,j+1}}{\Delta\eta^2}\eta_y^2 + \\ & \frac{\psi_{i+1,j} - \psi_{i-1,j}}{\Delta\xi}\xi_{yy} + \frac{\psi_{i,j+1} - \psi_{i,j-1}}{\Delta\eta}\eta_{yy}.\end{aligned} \tag{10}$$

Since the analytical formulas for $\xi(x, y)$ and $\eta(x, y)$ are known, one can take the necessary partial derivatives without having to make numerical approximations of them. The partial derivatives have been compiled in Tables 1 and 2.

x-Derivatives	
ξ_x	1
ξ_{xx}	0
η_x	$\frac{-y(h(x))_x}{(h(x))^2}$
η_{xx}	$-y\frac{(h(x))_{xx}h(x)-2((h(x))_x)^2}{(h(x))^3}$
$h(x)_x$	$\frac{\pi sin(\pi x)}{10}$
$h(x)_{xx}$	$\frac{\pi^2 cos(\pi x)}{10}$

Table 1: All the derivatives with respect to x used in order to compute the ψ derivatives in reference space.

y-Derivatives	
ξ_y	0
ξ_{yy}	0
η_y	$\frac{1}{h(x)}$
η_{yy}	0

Table 2: All the derivatives with respect to y used in order to compute the ψ derivatives in reference space.

If one removes the zero terms and then plugs the discretized partial derivatives from Eqns. 9

and 10 into Eqn. 3 to yield

$$\begin{aligned}\frac{\partial^2\psi}{\partial x^2}+\frac{\partial^2\psi}{\partial y^2}=&\frac{\psi_{i-1,j}-2\psi_{i,j}+\psi_{i+1,j}}{\Delta\xi^2}\xi_x^2+\\&2\frac{\psi_{i-1,j-1}+\psi_{i+1,j+1}-\psi_{i-1,j+1}-\psi_{i+1,j-1}}{4\Delta\xi\Delta\eta}\xi_x\eta_x\\&\frac{\psi_{i,j-1}-2\psi_{i,j}+\psi_{i,j+1}}{\Delta\eta^2}\eta_x^2+\\&\frac{\psi_{i,j+1}-\psi_{i,j-1}}{\Delta\eta}\eta_{xx}+\\&\frac{\psi_{i,j-1}-2\psi_{i,j}+\psi_{i,j+1}}{\Delta\eta^2}\eta_y^2=0.\end{aligned}\tag{11}$$

The partial derivatives in Tables 1 and 2 can then be evaluated at each grid point in order to turn those terms into constants. This allows Eqn. 11 to be used in order to solve for the the stream function by setting up a matrix-vector system, $\boldsymbol{A\Psi = F}$, where the partial derivatives end up being evaluated at every grid point in the reference space and becoming constant terms.

Task 2 - System Solving

A matrix-vector system was constructed in order to solve for $\psi(\xi,\eta)$ at all grid points. The **A**-matrix is a square, sparse matrix that is $N_{tot} \times N_{tot}$ in size. A N_{tot} loop was placed over this matrix in order to cycle over each row. Each row was then updated with the appropriate terms in each column such that the discretized PDE in Eqn. 11 held true. Once this matrix was constructed, the Python Scipy package was used to solve for $\psi(\xi,\eta)$. From there the stream function was manipulated to fit the desired needs of the problem such as contour mapping or velocity profiling.

Task 2 wants a print out of the results of this matrix-vector system for $r = 0$, and it can be found in Table 3. Additionally, it asks for contour maps of ψ for $r = 0$ and $r = 1$ which can be found in Figures 4 and 5, respectively.

ξ-Position	$\eta = 0$	$\eta = 0.25$	$\eta = 0.5$	$\eta = 0.75$	$\eta = 1$
$\xi = 0$	0.00000	0.25000	0.50000	0.75000	1.00000
$\xi = 0.0625$	0.00000	0.24650	0.49403	0.74417	1.00000
$\xi = 0.125$	0.00000	0.24578	0.49299	0.74348	1.00000
$\xi = 0.1875$	0.00000	0.24659	0.49444	0.74501	1.00000
$\xi = 0.25$	0.00000	0.24821	0.49718	0.74761	1.00000
$\xi = 0.3125$	0.00000	0.25026	0.50056	0.75071	1.00000
$\xi = 0.375$	0.00000	0.25247	0.50415	0.75394	1.00000
$\xi = 0.4375$	0.00000	0.25464	0.50765	0.75702	1.00000
$\xi = 0.5$	0.00000	0.25663	0.51083	0.75979	1.00000
$\xi = 0.5625$	0.00000	0.25833	0.51352	0.76211	1.00000
$\xi = 0.625$	0.00000	0.25962	0.51558	0.76388	1.00000
$\xi = 0.6875$	0.00000	0.26042	0.51685	0.76499	1.00000
$\xi = 0.75$	0.00000	0.26058	0.51715	0.76532	1.00000
$\xi = 0.8125$	0.00000	0.25992	0.51619	0.76464	1.00000
$\xi = 0.875$	0.00000	0.25820	0.51353	0.76252	1.00000
$\xi = 0.9375$	0.00000	0.25505	0.50848	0.75818	1.00000
$\xi = 1$	0.00000	0.25000	0.50000	0.75000	1.00000

Table 3: All the $\psi(\xi, \eta)$ values for the $r = 0$ solution.

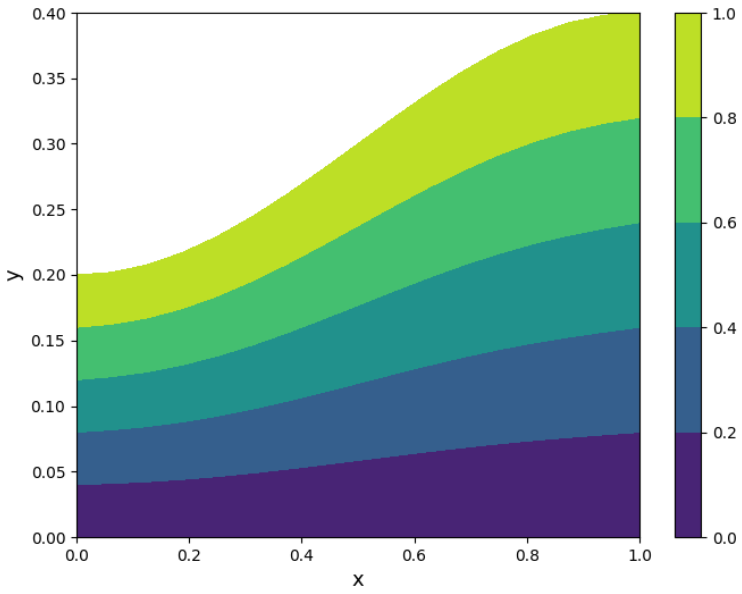

Figure 4: A contour mapping of the stream function for $r = 0$ with the same number of contours as points in the η direction.

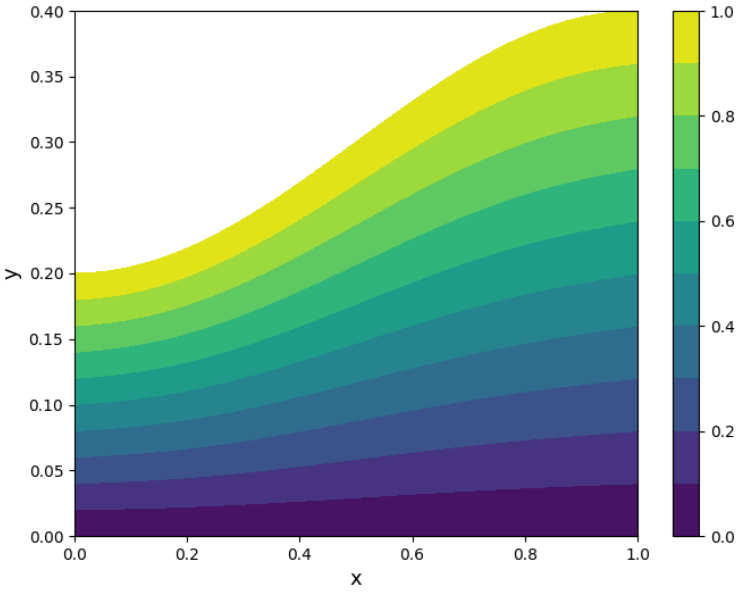

Figure 5: A contour mapping of the stream function for $r = 1$ with the same number of contours as points in the η direction.

There is not much of a difference between the two solutions with regards to ψ values, other than the higher r is, the more distinct levels there are in ψ. This makes sense because ψ is a linear function, so if the number of grid points is doubled vertically, the same doubling should occur to the number of streamlines in the contour plot as each streamline corresponds to a row of points. In this case, as r is incremented from 0 to 1, the figure gains four additional streamlines.

Task 3 - Tangential Velocity Profiling

Task 3 asks for a tangential velocity profiling along the top wall of the diffuser for three different r values: 0, 1, and 2. This profiling can be seen in Figure 6.

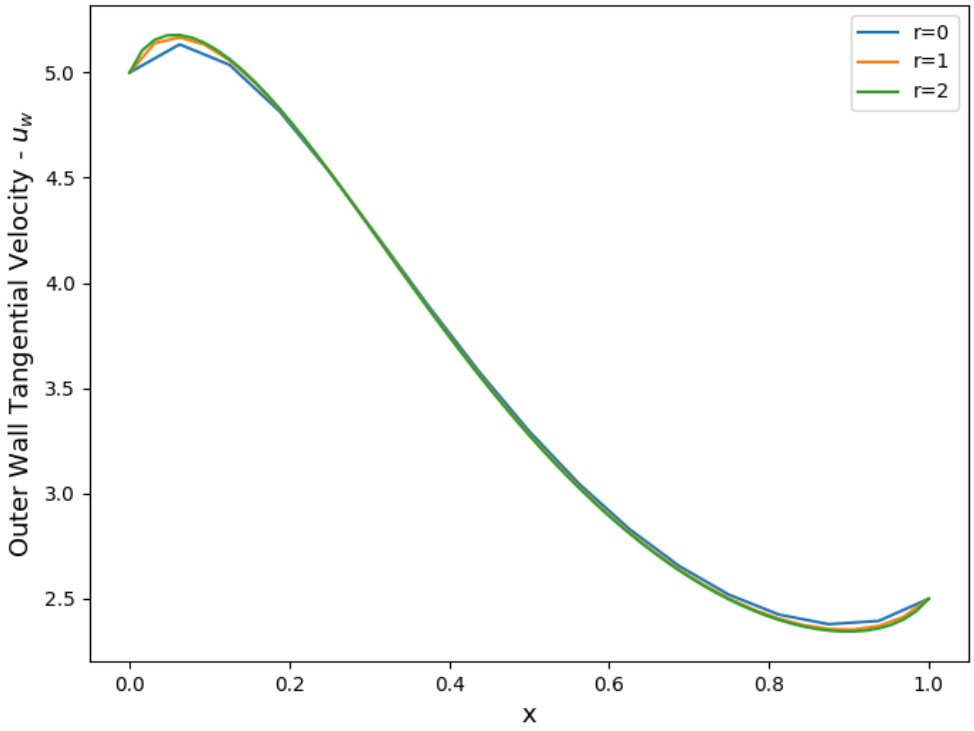

Figure 6: Caption

One of the biggest differences from the three iterations of profiling the tangential velocity is that one does not actually see the true maximum and minimum until r is increased. The $r = 0$ and $r = 1$ profiles fall short of the $r = 2$ maximum and minimum velocities. As r increases, the value converges towards the true solution and the results are able to get closer to the true minimum and maximum velocities along the wall.

Task 4 - Velocity Profiling

Task 4 asks for a velocity profile at showcasing $u(y)$ at $x = 0.25$, and at $x = 0.75$ with refinement index $r = 2$. These profiles can be seen in Figures 7 and 8.

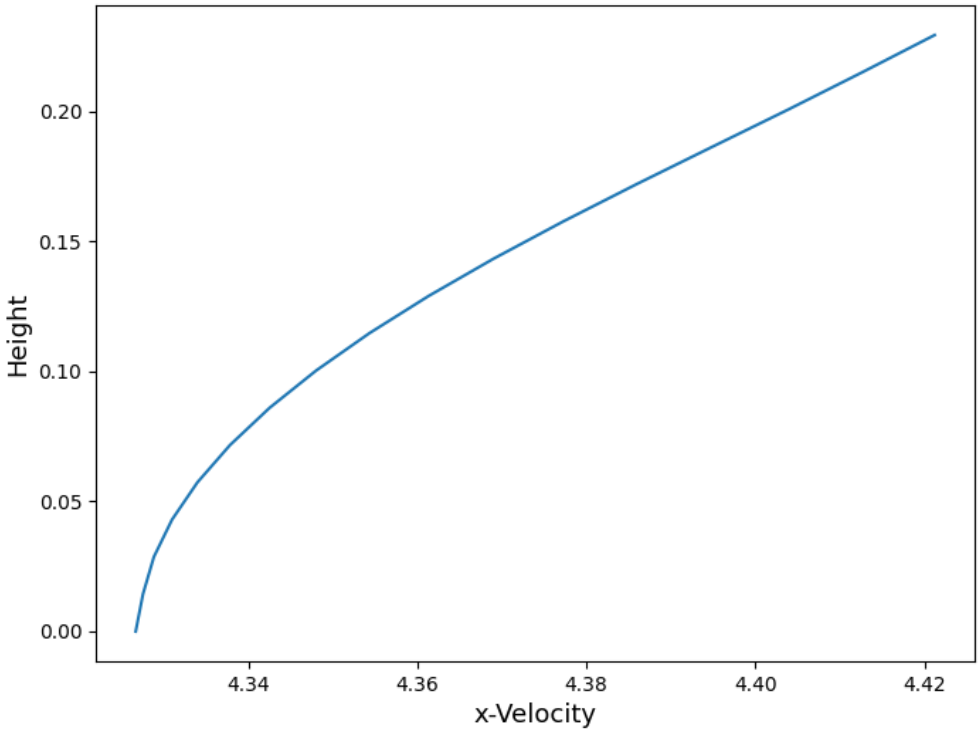

Figure 7: Towards the $x = 0$ mark of the diffuser, the x-velocity is increasing.

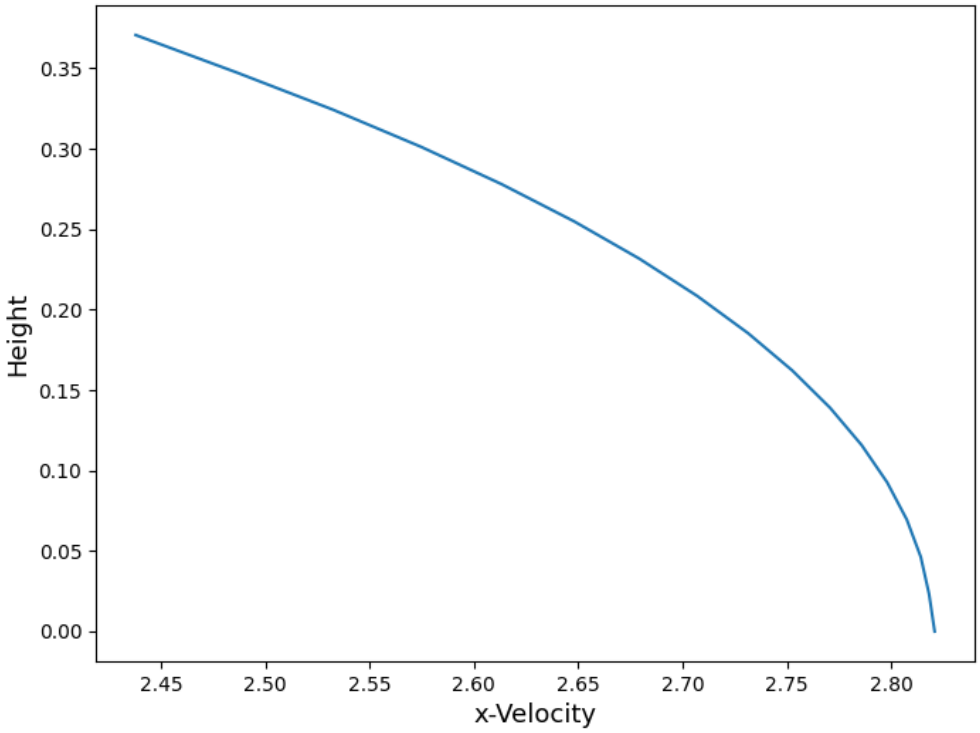

Figure 8: Further along the length of the diffuser at $x = 0.75$, the x-velocity decreases with height.

These results are consistent with what is expected. For an incompressible flow, $\rho u A = const.$ As the area of the diffuser, represented by the height $h(x)$, increases, the magnitude of the velocity should be decreasing, and if one looks at a magnitude contour map of the flow field like that in Figure 9, exactly this relationship is shown. The likely reason the x-velocity picks up at $x = 0.25$ is because of the increase in y-velocity near that point like the one seen in Figure 10.

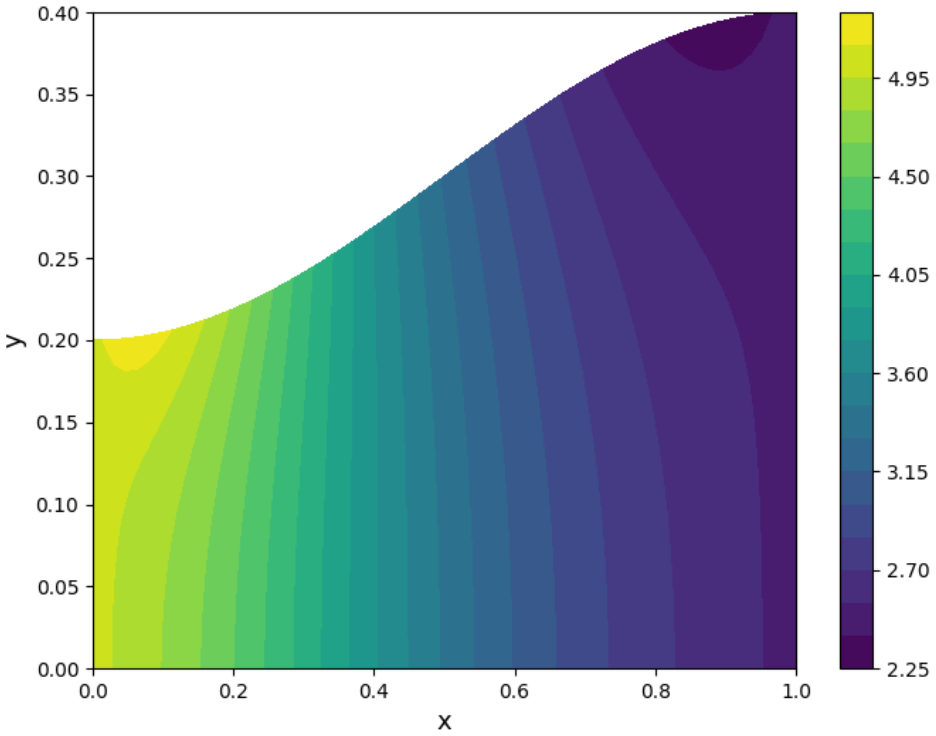

Figure 9: A contour plot of the magnitudes of the velocity field. As the area (represented by theight) increases, the overall velocity decreases.

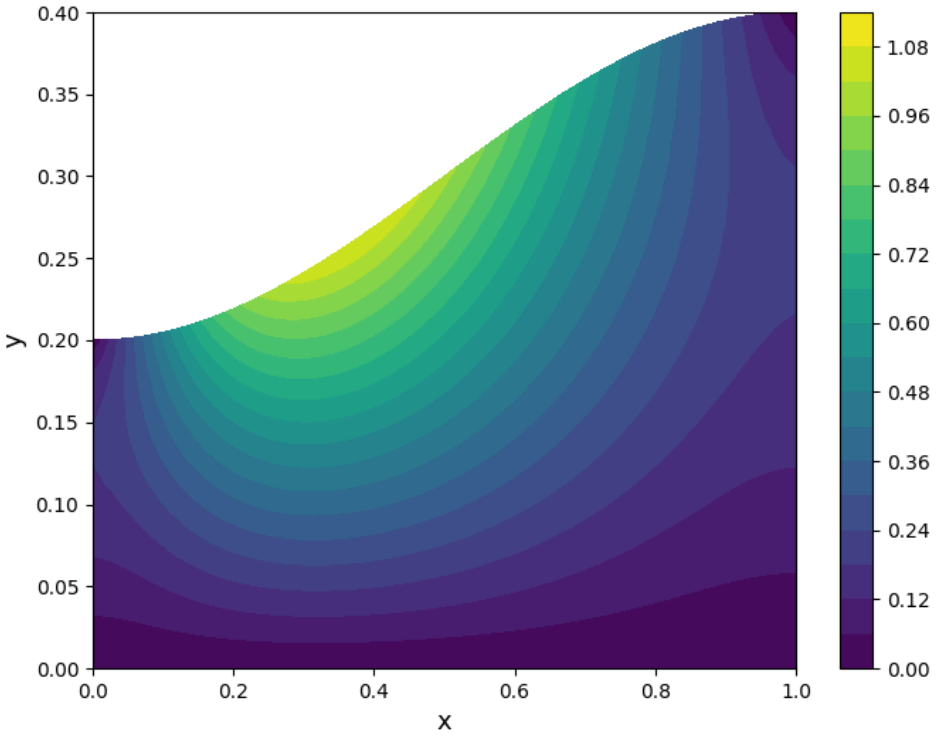

Figure 10: A contour map of the y-velocity for $r = 2$, notice the sharp increase in velocity near $x = 0.25$.

Due to the angled nature of the top wall, any fluid travelling vertically will be deflected, so the energy is rotated from the y-direction to the x-direction, causing a localized spike in x-velocity near $x = 0.25$. But overall, the trend does follow the continuity relationship as the x-velocity is decreasing along the length of the diffuser as evidenced by the drop in the average velocity from 4.4 at $x = 0.25$, to 2.6 at $x = 0.75$. This idea of the x-velocity dropping along the length of the diffuser is also reinforced visually by a contour mapping of the x-velocity like that in Figure 11.

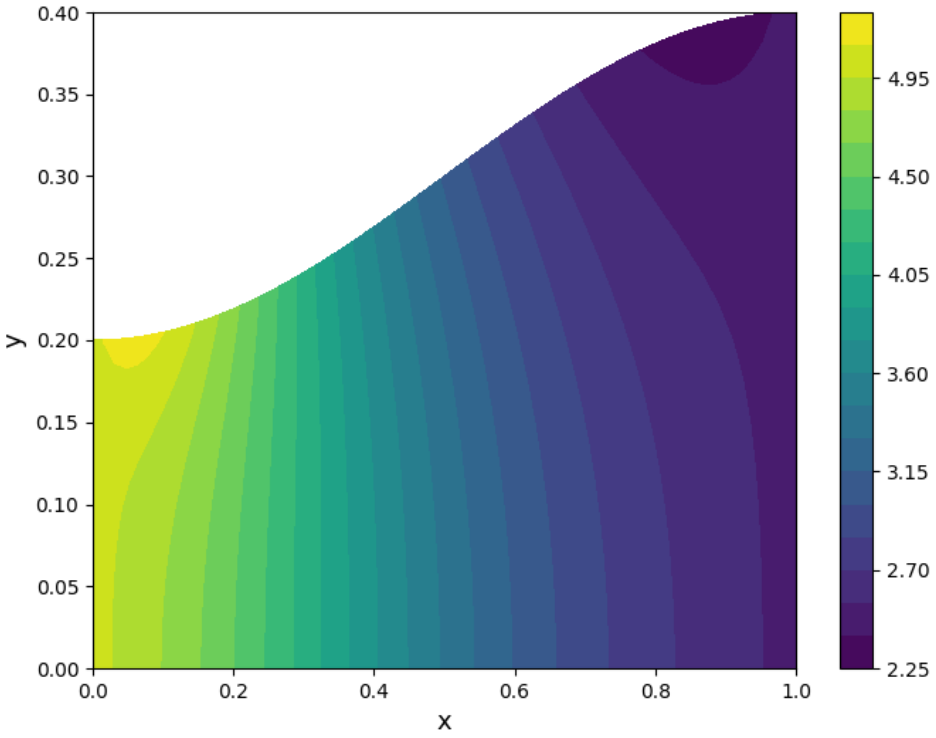

Figure 11: The average x-velocity decreases along the length of the contour.

Task 5 - Drag Coefficient Convergence Study

Task 5 involved performing a convergence study on the drag coefficient along the upper wall of the diffuser. This drag coefficient is described mathematically as

$$c_d = \frac{1}{L}\int_0^L c_p n_x dx, \tag{12}$$

where L is the length of length of diffuser n_x is the normal component in the x-direction, and c_p is the pressure coefficient which is defined as

$$c_p = 1 - \frac{u_w}{u_\infty}. \tag{13}$$

The study used $r = 0, 1, 2$, and using $r = 5$ as a reference for the "exact" drag coefficient and a convergence plot of the results can be seen in Figure 12.

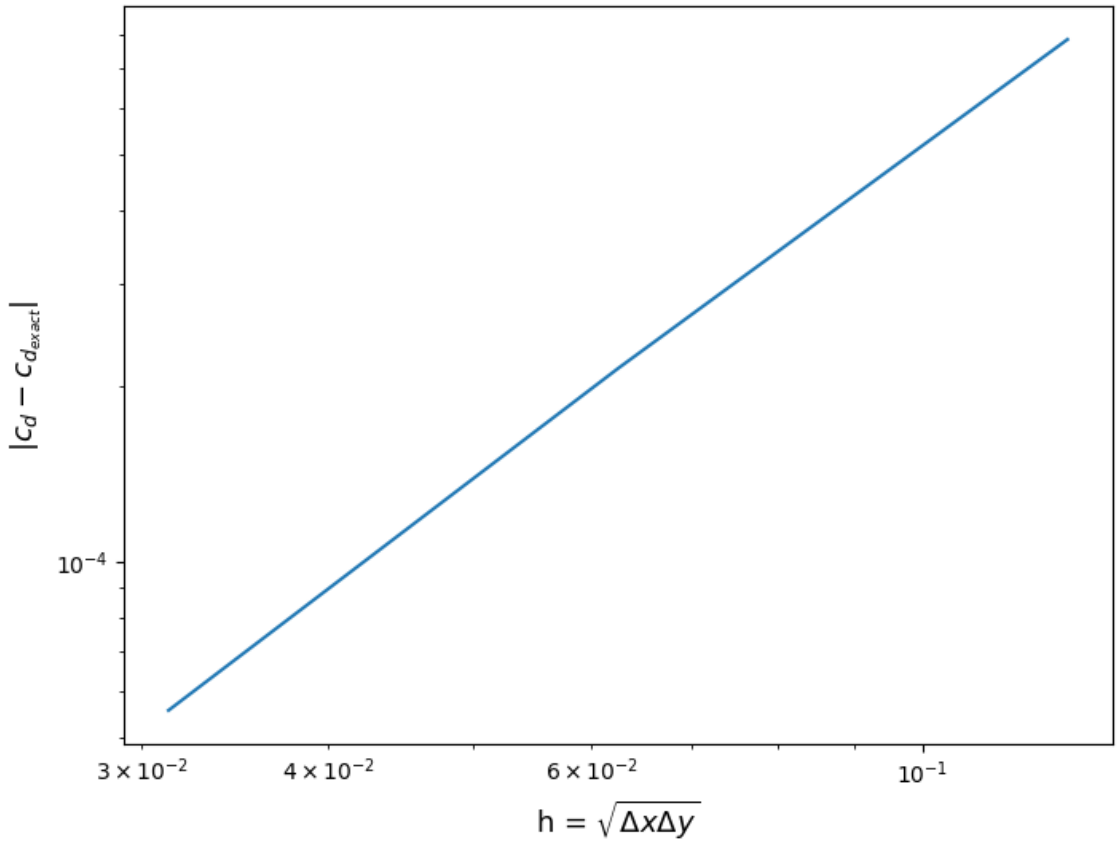

Figure 12: The convergence rate of the error in the drag coefficient is 2, which is expected

All of the FDM schemata used are second order accurate, so a convergence rate of approximately 2 is expected. Second order accuracy means that for every increase in the refinement index, N increases by a factor of two so the error should go down by a factor of four. When plotting the difference in errors on a loglog plot like of Figure 12, the slope should be ≈ 2, and Figure 12 has that with a slope of 1.911. This confirms the expectations of everything being second order accurate. The final result is that this diffuser has a drag coefficient of ≈ -0.0965.

REFERENCES

[1] Krzysztof Fidkowski. *Computational Fluid Dynamics*. University of Michigan, Aug. 2021, pp. 41–42, 44.

[2] Krzysztof Fidkowski. *Project 1: Flow in a Diffuser*. Sept. 2021.